Different topologies of natural vortex dislocations in Mode A wake

Cai Tian (田偲) ,[1] Zhaoyu Shi (史召宇) ,[2, a)] Fengjian Jiang (蒋奉兼) ,[3] and Helge I. Andersson[2]
[1)]*Department of Marine Technology, Norwegian University of Science and Technology (NTNU), NO-7491 Trondheim, Norway*
[2)]*Department of Energy and Process Engineering, NTNU, NO-7491, Trondheim, Norway*
[3)]*SINTEF Ocean, NO-7052, Trondheim, Norway*

(Dated: 12 January 2022)

The Mode A wake behind a circular cylinder at Reynolds number 200 was simulated by directly solving the three-dimensional Navier-Stokes equations (DNS). A more detailed investigation of different topologies of natural vortex dislocations in Mode A wake was systematically described. Besides the two-side natural vortex dislocation defined by Williamson ["The natural and forced formation of spot-like 'vortex dislocations' in the transition of a wake," J. Fluid Mech. 243, 393-441 (1992)], three new topologies of vortex dislocations were identified. Additionally, the formation process and mechanism of these newly identified dislocation topologies were addressed. The results in this Letter provide a more thorough understanding of the natural vortex dislocations in the Mode A wake.

Wake flow behind circular cylinders has been actively investigated for decades. For a long smooth circular cylinder under a steady uniform incoming flow, its wake is governed by the Reynolds number $Re = UD/\nu$ (where U represents the uniform inflow velocity, D is the length scale of the circular cylinder perpendicular to the inflow, and ν is the kinematic viscosity of the fluid). It is well-known that when Re exceeds 47, the steady and laminar wake flow transforms to the periodic two-dimensional vortex shedding flow[1]. As Re reaches 190, the wake flow transforms from two-dimensional to three-dimensional through the Mode A instability, which originates from the elliptic instability[2]. At 190<Re<193, a stable state of Mode A was first experimentally observed by C.H.K. Williamson[2] and confirmed by numerical studies[3–5]. The stable Mode A structure consists of two counter-rotating streamwise vortices forming a Mode A vortex loop with a wavelength around 4D in spanwise direction. At 193<Re<230, the stable Mode A becomes unstable and large-scale vortex dislocations (i.e., Mode A*) appears[2,4]. When Re further increases to above 230, Mode B[2,6], Mode C[7], and wake transition to turbulence[8–10] follow. To distinguish from the periodic forced vortex dislocation, which usually occurs in the wake behind an artificially designed nonuniform configuration, e.g., the step cylinder[11–17], the ring-attached cylinder[18], the cylinder with end-plates or mounted on a wall[19–21], etc., Williamson[18] defined the intermittent dislocation induced by Mode A instabilities as the natural vortex dislocation. According to previous studies[2,13,22], both the natural and forced vortex dislocations are mainly caused by the different shedding frequencies between the neighboring vortices. In the flow region where the natural vortex dislocation happens, it was found that the base suction and the shedding frequency decrease while the vortex formation length increases[2,22].

Although many previous studies have widely characterized the three-dimensional instability in the Mode A wake, the investigations of different topologies of natural vortex dislocations in the Mode A flow regimes and their formation mechanisms are still limited. To the best of our knowledge, only the two-side natural vortex dislocation, i.e., vortex dislocation happens simultaneously at two sides of the slowly shed vortex, has been reported in the existing experimental and numerical studies[2–4,22,23].

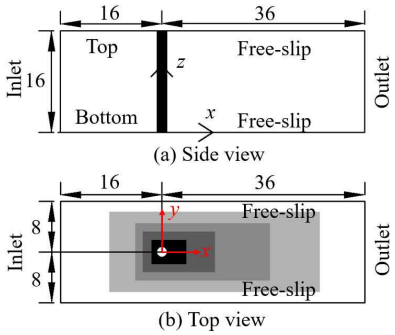

FIG. 1. Computational domain and coordinate system: (a) Side view, (b) Top view. The three directions are named streamwise ($x-$direction), crossflow ($y-$direction) and spanwise ($z-$direction). In panel (b), the grid refinement regions are schematically illustrated at top $xy-$plane of the domain and marked with darker shades of grey for finer regions. The length unit is the cylinder diameter D.

The primary aim of the present Letter is to investigate the natural vortex dislocations in the Mode A cylinder wake in detail. To achieve this, the flow past a circular cylinder at $Re =$ 200 was studied by using a well-validated[24–26] Direct Numerical Simulation (DNS) code *MGLET*[27] to directly solve the three-dimensional Navier-Stokes equations. In Fig. 1, the computational domain and coordinate system are shown. The origin is located in the center of the cylinder bottom. For the flow domain, the inlet and outlet are located at 16D and 36D from the cylinder axis, respectively. The distance between the top and bottom is 16D, which is equal to the length of the cylinder. These parameters are comparable to those used in the previous studies[4,5] for modeling cylinder wake with the similar $Re_D \approx 200$. A dimensionless constant velocity U is applied at the inlet. The outlet is prescribed by Neumann and

a)Author to whom correspondence should be addressed. Electronic mail: zhaoyu.shi@ntnu.no

zero-pressure conditions. The other four boundaries are set up as free-slip walls. On the surface of the circular cylinder, the no-slip and impermeability conditions are used. MGLET uses a staggered Cartesian grid and interpolates the solid geometry through an immersed boundary method[28]. Around the cylinder, a local refinement of the grid is achieved by embedding zonal grids[27]. A schematic illustration of the grid design in the x- and y-direction is schematically illustrated in Fig. 1(b). The grid is homogeneous and equal to the finest resolution in the spanwise direction. A constant time step is used to ensure a CFL (Courant-Friedrichs-Lewy) number smaller than 0.5. Three cases with the decreasing finest resolution, i.e., $0.02D$, $0.015D$, and $0.01D$, have been simulated for grid convergence study. All phenomena and mechanisms discussed in the present Letter are detected in these three cases. The results from the case with the grid resolution $0.01D$ are presented in the following. Moreover, by examining all new findings of the present Letter in another simulation with the same numerical settings, the grid resolution $0.01D$, but a longer cylinder of length $24D$, the spanwise length convergence study proves that the following discussions can be representative of an infinitely long circular cylinder as long as the flow field in the vicinity of the spanwise boundaries is discarded.

Based on long-time observations (around 280 shedding periods), mainly two topologies of natural vortex dislocations are identified: (1) two-side natural vortex dislocation ($2sVD$) and (2) one-side natural vortex dislocation ($1sVD$). Examples of vortex interactions with these two topologies of vortex dislocations are illustrated by the consecutive snapshots of the isosurface of λ_2 and streamwise vorticity ($\omega_x = \partial w/\partial y - \partial v/\partial z$) in the first row of Figs. 2, 3, 5, and 6. The corresponding schematic topology sketches are plotted in the second row of these figures, where the gray and black lines represent the vortex tube shedding from the +Y and –Y sides of the circular cylinder, respectively. All vortices are labeled by a combination of capital letters and numbers: 'U', 'M', and 'L' represent the vortices in the upper, middle, and lower flow regions, respectively, while the number indicates the shedding order in each selected dislocation process. The red and blue curves mark the positive and negative streamwise vortices, respectively. One can see that, in both the one-side and two-side natural vortex dislocation processes, three vortex cells can be identified: U-, M-, and L-cell vortices. The two-side natural vortex dislocation is defined when an M-cell vortex dislocates simultaneously with its corresponding U- and L-cell vortices. When vortex dislocations only appear at U-M or L-M boundaries, we call it one-side natural vortex dislocation. To ease the observation, we only show the streamwise vorticities involved in vortex dislocation processes.

The two-side natural vortex dislocations are divided into two sub-topologies, distinguished by whether or not sustainable clear loop structures evolve in the middle flow region. Fig. 2 shows the first sub-topology ($2sVDa$), which is the conventional two-side natural vortex dislocation defined in Ref. 18. It is evidently observed that, when the M-cell vortices in Figs. 2(c) and (e) dislocate with their corresponding U- and L-cell vortices, the formed loop structures M2 and M'3 can exist in the flow region $x/D > 5D$ in Figs. 2(e) and (g). However, when the spanwise length of the M-cell vortices in Figs. 3(c) and (e) become short (around $1D$), the formed loop structure M2 and M'3 dissipate in the near wake ($x/D < 5$) after they form and shed from the shear layer in Figs. 3(e) and (g). We call it the second sub-topology of two-side natural vortex dislocation ($2sVDb$). A common feature of $2sVDa$ and $2sVDb$ is that their induced vortex loop structures consist of a pair of counter-rotating streamwise vortices compared to the corresponding streamwise components of a common Mode A vortex loop[2]. As highlighted by the red rectangle in Figs. 2(d) and 3(d), a two-side dislocation loop on the -Y side of cylinder consists of a negative upper streamwise vortex and a positive lower streamwise vortex. In contrast, a Mode A vortex loop on the -Y side consists of a positive upper streamwise vortex and a negative lower streamwise vortex, as highlighted by the red rectangle in Fig. 3(b). The corresponding mechanism is illustrated in Fig. 4, where the subplot (a) is reproduced from Ref. 2. It shows that when a Mode A loop structure forms without dislocation, the upper and lower ends of the Mode A vortex loop on the -Y side bend towards the downstream direction. This makes the loop itself consist of an upper-side positive and a lower-side negative streamwise vortex. On the other hand, as shown in Fig. 4(b), when a two-side dislocation ($2sVD$) happens, the formed vortex loop bends into the upstream direction in an opposite way to the Mode A loop shown in Fig. 4(a). The different bent directions in the Mode A loop and the two-side dislocation loop cause their different compositions of streamwise vortices.

As shown in Figs. 5 and 6, the one-side natural vortex dislocation ($1sVD$) arises either between the U- and M-cell vortices or between the M- and L-cell vortices. Meanwhile, the dislocation-induced streamwise vortices only form on one side of the M-cell vortices in $1sVD$, instead of emerging on both sides of the M-cell vortices, similarly to what occurs in $2sVD$. As a result, there is no clear loop structure forming in $1sVD$.

Although the vortex interactions in the one- and two-side dislocation are different, both two topologies of dislocations are attributed to the same physical mechanism, i.e., the increased phase difference between the dislocated vortex cells. From Fig. 3(a), one can see that the main vortex tubes behind the circular cylinder in Mode A are spanwise vortices. This means that the variation of the streamwise distance between different vortex cells can reflect the changes in their phase difference. In the present study, we use the location of the most concentrated spanwise vorticity to indicate the position of the corresponding vortex. The same method was introduced and used in Ref. 13. In the first and second lines of Table I, one can see that from the early stage of $2sVDb$ to the moment when dislocation happens ($tU/D = 286.4$), the streamwise distance between the M-cell vortices and the corresponding U- and L-cell vortices increases from $0.3D \sim 0.4D$ to $2.0D \sim 2.2D$. By using the same method, the similar phase increment for the three other vortex dislocations is also found in Table I.

The time variations of the shedding frequencies in different dislocation processes are presented in Fig. 7, where the instantaneous shedding frequency of U-cell vortex ($f_U D/U$), M-cell vortex ($f_M D/U$), and L-cell vortex ($f_L D/U$) are esti-

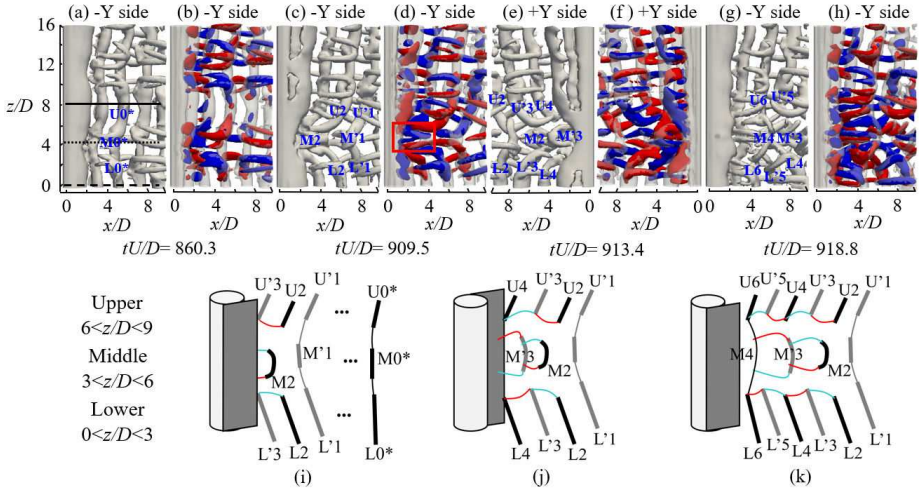

FIG. 2. (a)-(h) Isosurfaces of $\lambda_2 = -0.001$ aside by the isosurfaces of $\omega_x = \pm 0.5$ ($+\omega_x$ in red and $-\omega_x$ in blue) illustrating the developments of vortex structures in the first sub-topology of two-side natural vortex dislocation ($2sVDa$). (i)-(k) Schematic topology illustrating the development of $2sVDa$. In panel (a), the black solid line at $z/D = 8.0$, the black dotted line at $z/D = 4.0$, and the black dashed line at $z/D = 0.0$ indicate the spanwise positions of time variations of shedding frequency given in Fig. 7(b).

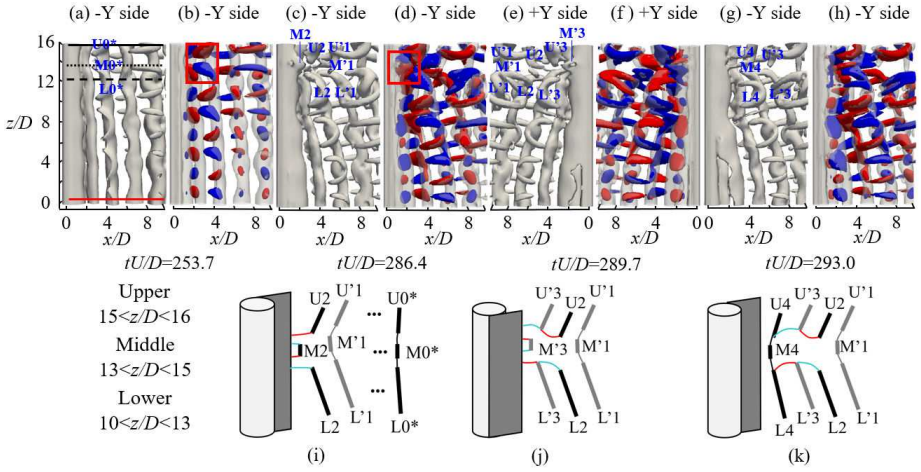

FIG. 3. (a)-(h): same as Fig. 2, but in the second sub-topology of two-side natural vortex dislocation ($2sVDb$). (i)-(k) Schematic topology. In panel (a), the black solid line at $z/D = 16.0$, the black dotted line at $z/D = 13.8$, the black dashed line at $z/D = 12.0$, and the red solid line at $z/D = 0$ indicate the spanwise positions of time variation of shedding frequency given in Fig. 7(a).

mated by using the time variation of the cross-flow velocity component (v/U) at the sampling point in the corresponding flow regions. The locations of these sampling points are illustrated in Figs. 2(a), 3(a), 5(a) and 6(a). The same approach was also used in Ref. 20. One can see that, in both $1sVD$ and $2sVD$, f_M (the red curve) is lower than f_U(the yellow curve) and f_L (the blue curve). Furthermore, when approaching the dislocation period which is highlighted by the red solid timeline, the shedding frequency difference between the M-cell vortex and its neighboring U- and L-cell vortices reaches its

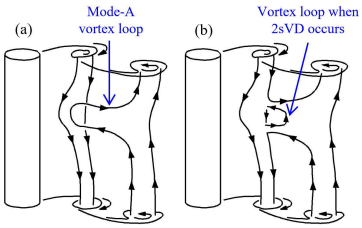

FIG. 4. Physical mechanism (a) to produce vortex loops of mode A (image reproduced with permission from J. Fluid. Mech. 328, 345-407 (1996). Copyright 1996 Cambridge University Press), (b) to produce vortex loops in the two-side vortex dislocation.

maximum value range. After dislocation finished, f_M, f_U, and f_L return to the same level.The similar phenomena were also reported in Ref. 22, but only for the conventional two-side natural vortex dislocation ($2sVDa$). It is the different shedding frequencies of the U-, M-, and L-cell vortices that cause the accumulation of the phase difference between them.

To explain why the similar phase accumulation mechanism can cause different topologies of natural vortex dislocations, we introduce the phrase 'initial phase difference' which is defined as the phase difference between the corresponding vortex cells at the early stage of a vortex dislocation process. As shown in Table I, at the early stage of $2sVDa$ and $2sVDb$, the initial phase differences of the U-M and M-L vortex pairs are close to each other. Therefore, when the M-cell vortex sheds slower during the vortex dislocation periods shown in Figs. 7(b) and (a), the M-cell dislocates with its counterpart U- and L-cell vortices simultaneously. However, when $1sVD$ just occurs, the phase difference of the vortex pair whose one-to-one relation will not be able to persist due to vortex dislocations is obviously larger than the phase difference of the other vortex pair. For example, at the early stage of $1sVDa$ ($tU/D = 1263.8$) in Fig. 5(a), the streamwise distance between $U0^*$ and $M0^*$ is -1.4 and that between the $L0^*$ and $M0^*$ is 1.6 as shown in the third row of Table I. This means that the initial phase difference of the U-M vortex pair is much smaller than that of the L-M vortex pair in this $1sVDa$. From $tU/D = 1263.8$ to 1288.7, due to the lower shedding frequency in the M-cell region compared to the U- and L-cell regions as shown in Fig. 7(c), X_{UM} and X_{LM} increase simultaneously from -1.4 to 1.8 and from 1.6 to 4.0, respectively. The increased distances are close for these two vortex pairs. In other words, during this period, the accumulated phase differences of U-M and L-M vortex pairs are at the same level. However, due to the different initial phase difference, when the M-cell vortex M3 dislocates with the corresponding L-cell L3 vortex at $tU/D = 1290.2$ in Fig. 5(c) the one-to-one relation between the U-cell vortex U3 and its counterpart M-cell vortex M3 still exists after the similar accumulated phase difference. In general, it is the discrepancy between the initial phase difference of the corresponding vortex pairs that induces the formation of $1sVD$.

The mechanism of the initial phase difference can be explained by examining the two-side vortex dislocation process shown in Fig. 3 and the corresponding time trace of the shedding frequency of different vortex cells in Fig. 7(a). As approaching the dislocation period, St_M gradually decreases from 0.197 to 0.181. Meanwhile, St_U and St_L also decrease, but at a smaller rate compared to St_M. However, the purple curve in Fig. 7(a) which represents the shedding frequency in the flow region far away from the dislocation region has a much slower decreasing rate comparing to the other curves. Overall, the farther away from the dislocated region, the smaller the decreasing rate of shedding frequency will be. As a result, after $2sVDb$ is completed in Fig. 3(e), the phase difference between the vortices in the flow regions $8 < z/D < 16$ and $0 < z/D < 8$ is not zero. This non-zero phase difference will become the initial phase difference in the subsequent vortex dislocation process. The different variation rates of shedding frequencies also appear in the other dislocation processes as shown in Figs. 2, 5, 6 and 7(b-d). This means that all topologies of vortex dislocation are able to induce the initial phase difference for the subsequent dislocation processes.

TABLE I. The streamwise distance between the corresponding U- and M-cell vortices ($x_{UM} = (x_U - x_M)/D$), and between the corresponding L- and M-cell vortices ($x_{LM} = (x_L - x_M)/D$) in the early stage (E) and vortex dislocation moment (VD) in the dislocation processes shown in Figs. 3, 2, 5, and 6.

Vortex dislocation	tU/D	x_{UM}	x_{LM}
$2sVDb$	253.7 (E)	0.3	0.4
	286.4 (VD)	2.0	2.2
$2sVDa$	860.3 (E)	0.8	0.6
	909.5 (VD)	2.4	2.2
$1sVDa$	1263.8 (E)	-1.4	1.6
	1288.7 (VD)	1.8	4.0
$1sVDb$	1294.7 (E)	1.5	-0.8
	1303.4 (VD)	2.9	0.3

In summary, our present results show a good agreement with previous studies, including the vortex dislocation mechanism[2,13,22] and the frequency variation during the natural vortex dislocation process[22]. More importantly, the numerical results provide more detailed information about the natural vortex dislocation process. The new findings are as follows:

- Three flow regions are defined in every vortex dislocation process, i.e., the upper, middle and lower flow regions, where three vortex cells, i.e., the U-, M-, and L-cell vortices are identified.
- According to whether vortex dislocations simultaneously appear at the U-M and M-L boundaries or not, two topologies of dislocation are identified, i.e., the two-side natural vortex dislocation ($2sVD$) and the one-side natural vortex dislocation ($1sVD$).
- Two sub-topologies of vortex dislocation are introduced in both $2sVD$ and $1sVD$: besides the conventional

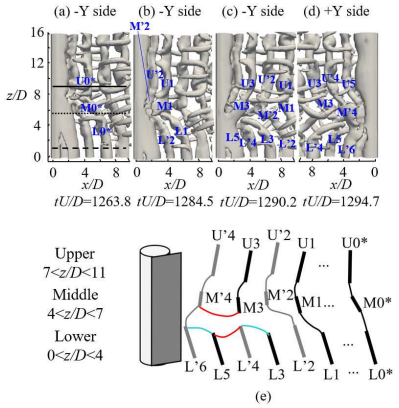

FIG. 5. (a)-(d) are the same as Fig. 2, but in the first sub-topology of one-side natural vortex dislocation (1*sVDa*). (e) Schematic topology illustrating the development of 1*sVDa*. In panel (a), the black solid line at $z/D = 9.0$, the black dotted line at $z/D = 5.4$, and the black dashed line at $z/D = 1.0$ indicate the positions of time traces of shedding frequency given in Fig. 7(c).

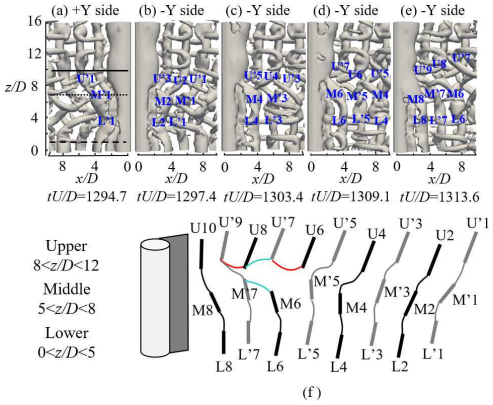

FIG. 6. (a)-(e) are the same as Fig. 2, but in the second sub-topology of one-side natural vortex dislocation (1*sVDb*). (f) Schematic topology illustrating the development of 1*sVDb*. In panel (a), the black solid line at $z/D = 10.0$, the black dotted line at $z/D = 7.0$, and the black dashed line at $z/D = 1.0$ indicate the positions of time traces of shedding frequency given in Fig. 7(d).

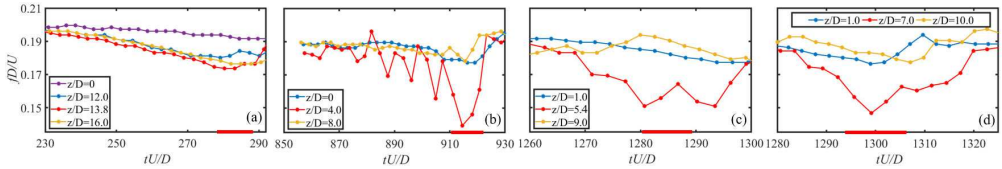

FIG. 7. (a)-(d) Time traces of the shedding frequency fD/U in the S-cell region (the yellow curve), St_M (the red curve), and St_L (the blue curve) corresponding to the frequency of the U-, M-, and L-cell vortices in the vortex dislocations shown in Fig. 3, 2, 5, and 6. In the timeline axis, the red thick line highlights the time period when vortex dislocation happens. In panel (a), the purple curve shows the time trace of the Strouhal number of vortices located in the flow region far away from the N-cell vortices.

two-side natural vortex dislocation (2*sVDa*), three new topologies of dislocations, i.e., 2*sVDb*, 1*sVDa*, and 1*sVDb*, are identified.

- The time traces of shedding frequency in different flow regions clearly show that both 2*sVD* and 1*sVD* are caused by lower shedding frequency in the M-cell region compared to that in the U- and L-cell regions. Moreover, after a vortex dislocation finishes, the unsynchronized variation of the shedding frequency in the U-, M-, and L-cell regions causes the non-zero phase difference between these flow regions, which becomes the initial phase difference of the subsequent vortex dislocation process and determines whether 2*sVD* or 1*sVD* occurs.

ACKNOWLEDGMENTS

Computing resources were granted by the Norwegian Research Council (Program for Supercomputing) under projects nn9352K and nn2649k.

[1]C. H. K. Williamson, "Vortex dynamics in the cylinder wake," Annu. Rev. Fluid Mech. **28**, 477–539 (1996).
[2]C. H. K. Williamson, "Three-dimensional wake transition," J. Fluid Mech. **328**, 345–407 (1996).
[3]S. Behara and S. Mittal, "Wake transition in flow past a circular cylinder," Phys. Fluids **22**, 114104 (2010).
[4]H. Jiang, L. Cheng, S. Draper, H. An, and F. Tong, "Three-dimensional direct numerical simulation of wake transitions of a circular cylinder," J. Fluid Mech. **801**, 353–391 (2016).
[5]H. Jiang, L. Cheng, F. Tong, S. Draper, and H. An, "Stable state of mode A for flow past a circular cylinder," Phys. Fluids **28**, 104103 (2016).
[6]H. Jiang and L. Cheng, "Strouhal–Reynolds number relationship for flow past a circular cylinder," J. Fluid Mech. **832** (2017).
[7]H. Jiang and L. Cheng, "Transition to chaos in the cylinder wake through the Mode C flow," Phys. Fluids **32**, 014103 (2020).
[8]F. S. Pereira, G. Vaz, L. Eça, and S. S. Girimaji, "Simulation of the flow

around a circular cylinder at Re= 3900 with Partially-Averaged Navier-Stokes equations," Int. J. Heat Fluid Flow **69**, 234–246 (2018).
[9]V. M. Molochnikov, N. I. Mikheev, A. N. Mikheev, A. A. Paereliy, N. S. Dushin, and O. A. Dushina, "SIV measurements of flow structure in the near wake of a circular cylinder at Re= 3900," Fluid Dyn. Res. **51**, 055505 (2019).
[10]G. Tian and Z. Xiao, "New insight on large-eddy simulation of flow past a circular cylinder at subcritical Reynolds number 3900," AIP Adv. **10**, 085321 (2020).
[11]C. Tian, F. Jiang, B. Pettersen, and H. I. Andersson, "Numerical investigation of flow around a step cylinder," in *Proceedings of 9th National Conference on Computational Mechanics (CIMNE), Trondheim, Norway, May 11-12* (2017) pp. 369–384.
[12]C. Tian, F. Jiang, B. Pettersen, and H. I. Andersson, "Antisymmetric vortex interactions in the wake behind a step cylinder," Phys. Fluids **29**, 101704 (2017).
[13]C. Tian, F. Jiang, B. Pettersen, and H. I. Andersson, "Vortex dislocation mechanisms in the near wake of a step cylinder," J. Fluid Mech. **891** (2020).
[14]C. Tian, F. Jiang, B. Pettersen, and H. I. Andersson, "Diameter ratio effects in the wake flow of single step cylinders," Phys. Fluids **32**, 093603 (2020).
[15]C. Morton and S. Yarusevych, "Vortex shedding in the wake of a step cylinder," Phys. Fluids **22**, 083602 (2010).
[16]Y. Yan, C. Ji, and N. Srinil, "Three-dimensional flip-flopping flow around a pair of dual-stepped circular cylinders in a side-by-side arrangement," Phys. Fluids **32**, 123608 (2020).
[17]J. McClure, C. Morton, and S. Yarusevych, "Flow development and structural loading on dual step cylinders in laminar shedding regime," Phys. Fluids **27**, 063602 (2015).
[18]C. H. K. Williamson, "The natural and forced formation of spot-like 'vortex dislocations' in the transition of a wake," J. Fluid Mech. **243**, 393–441 (1992).
[19]C. H. K. Williamson, "Oblique and parallel modes of vortex shedding in the wake of a circular cylinder at low Reynolds numbers," J. Fluid Mech. **206**, 579–627 (1989).
[20]S. Behara and S. Mittal, "Flow past a circular cylinder at low Reynolds number: Oblique vortex shedding," Phys. Fluids **22**, 054102 (2010).
[21]S. Mittal, J. Pandi, and M. Hore, "Cellular vortex shedding from a cylinder at low Reynolds number," J. Fluid Mech. **915**, A74 (2021).
[22]M. Braza, D. Faghani, and H. Persillon, "Successive stages and the role of natural vortex dislocations in three-dimensional wake transition," J. Fluid Mech. **439**, 1–41 (2001).
[23]S. C. Luo, Y. T. Chew, and Y. T. Ng, "Characteristics of square cylinder wake transition flows," Phys. Fluids **15**, 2549–2559 (2003).
[24]F. Jiang, B. Pettersen, and H. I. Andersson, "Turbulent wake behind a concave curved cylinder," J. Fluid Mech. **878**, 663–699 (2019).
[25]U. Jenssen, W. Schanderl, C. Strobl, L. Unglehrt, and M. Manhart, "The viscous sublayer in front of a wall-mounted cylinder," J. Fluid Mech. **919**, A37 (2021).
[26]C. Tian, F. Jiang, B. Pettersen, and H. I. Andersson, "Vortex system around a step cylinder in a turbulent flow field," Phys. Fluids **33**, 045112 (2021).
[27]M. Manhart, "A zonal grid algorithm for DNS of turbulent boundary layers," Comput. Fluids **33**, 435–461 (2004).
[28]N. Peller, A. L. Duc, F. Tremblay, and M. Manhart, "High-order stable interpolations for immersed boundary methods," Int. J. Numer. Meth. Fl. **52**, 1175–1193 (2006).

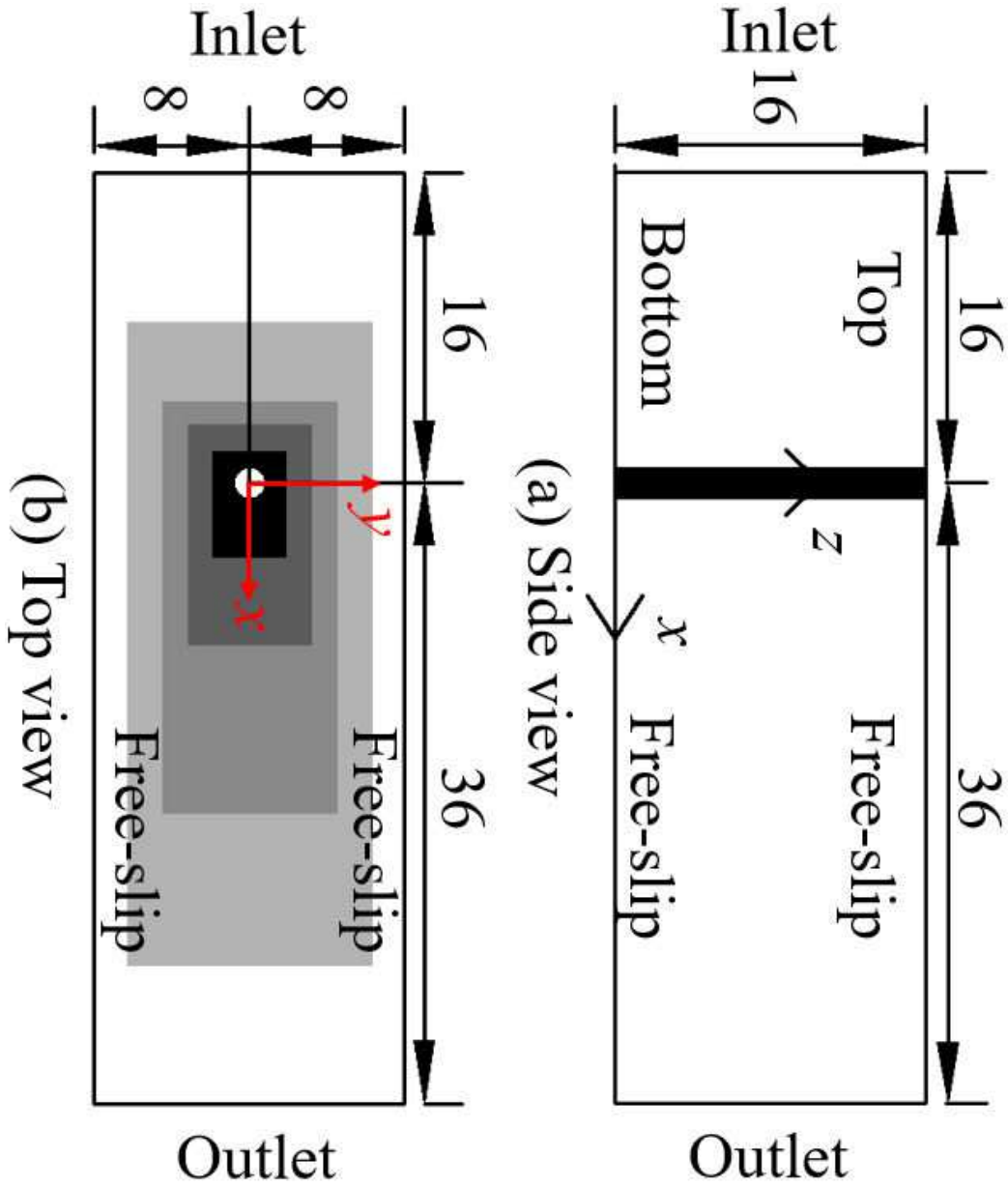

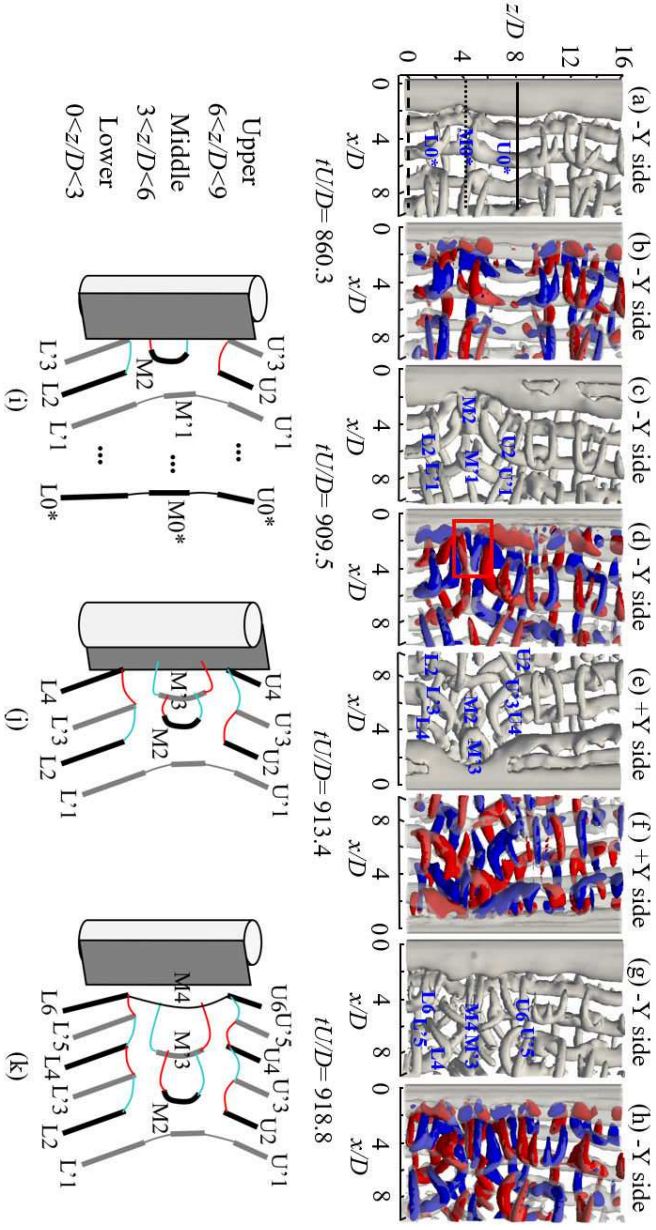

Physics of Fluids

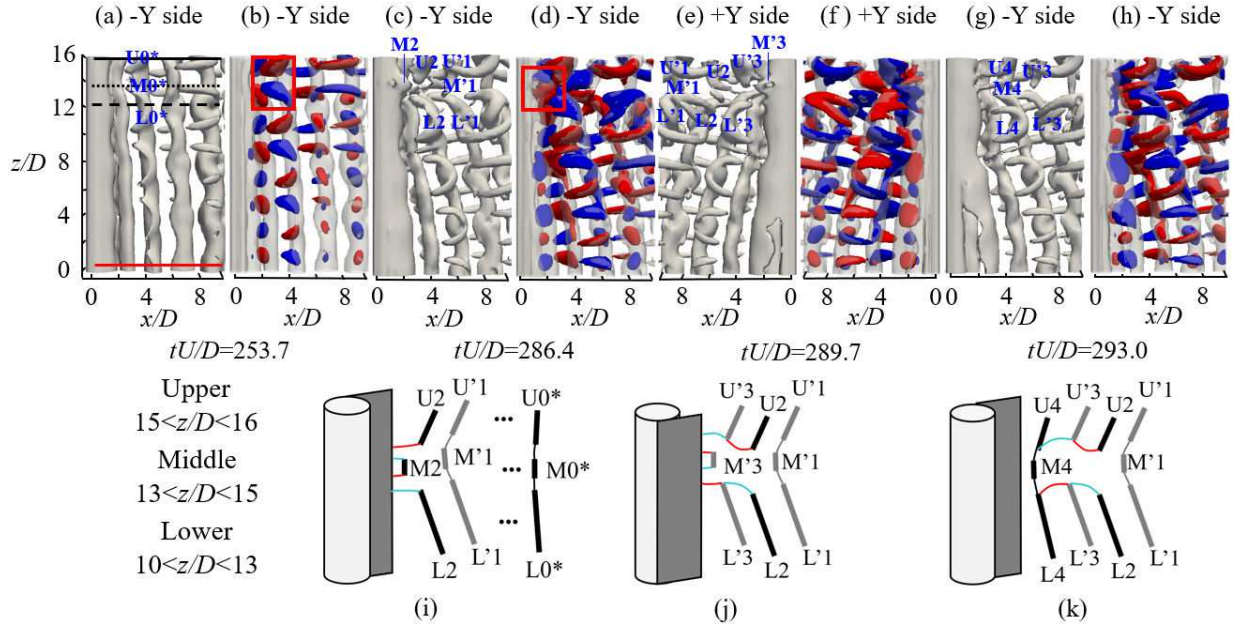

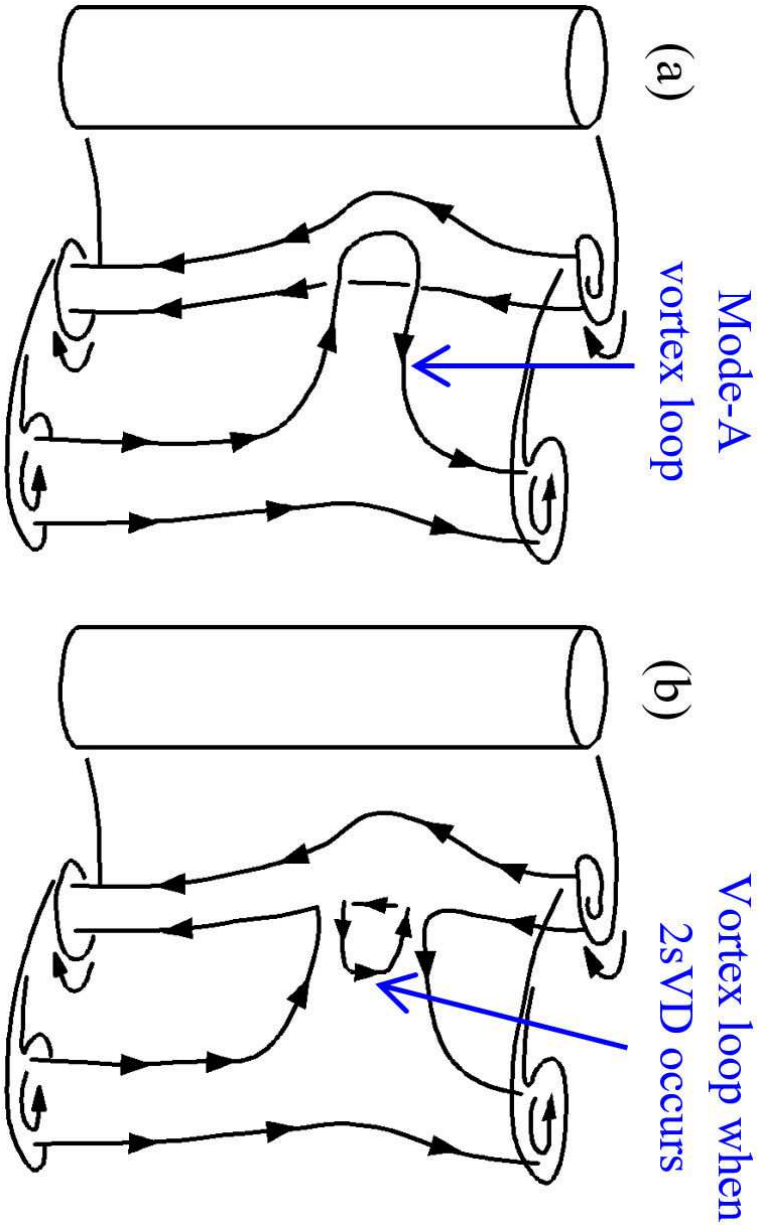

Physics of Fluids